ACS OMEGA

http://pubs.acs.org/journal/acsodf

Article

Hysteresis Dynamic Modeling and Analysis of Flexible Nano Silver–Polyvinyl Alcohol Humidity Sensor Based on the Microscopic Process and Langmuir–Fick Theory

Jie Xia,[‖] Xuepei Wang,[‖] Xiang Wang, Krisztina Majer-Baranyi, and Xiaoshuan Zhang*

Cite This: *ACS Omega* 2022, 7, 14994–15004

Read Online

ACCESS | Metrics & More | Article Recommendations | Supporting Information

ABSTRACT: In recent years, advances in materials science and manufacturing technologies have facilitated the development of flexible sensors. However, there are still performance gaps between emerging flexible sensors and traditional silicon-based rigid sensors, especially lacking dynamic modeling and optimization analysis for addressing above challenges. This paper describes a hysteresis dynamic modeling method for flexible humidity sensors. Through inkjet printing and coating methods, the polyvinyl alcohol (PVA) sensitive layer and nano silver interdigital electrode are fabricated on flexible polyethylene naphthalate substrates. The performance characterization results show that the sensitivity and maximum hysteresis within the range of 12−98% relative humidity (RH) are −0.02167 MΩ/% RH and 2.7% RH, respectively. The sensor also has outstanding dynamic response ability and stability in a wide range of humidity variation. The hysteresis mechanism of flexible humidity sensors is theoretically analyzed from microscopic hysteresis processes, Langmuir monomolecular adsorption dynamic modeling, and Fick diffusion dynamic modeling. These hysteresis models provide a path for the hysteresis optimization of flexible PVA humidity sensors. Further exploration of the diffusion rate of water molecules and the proportion of PVA in ink represents promising hysteresis optimization directions of flexible humidity sensors based on PVA-sensitive material.

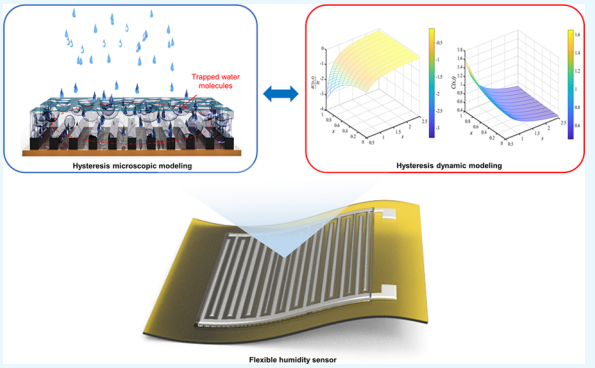

1. INTRODUCTION

Humidity sensors, as a device to sense humidity and convert it into an output signal according to certain rules, have been widely used in various fields including industrial production,[1] environmental monitoring,[2] precision agriculture,[3] health care,[4] wearable devices,[5] and internet of things.[6] As a non-smooth and memoryless phenomenon, hysteresis is a common problem in the humidity sensor application based on adsorption and desorption, and it is particularly prominent in the humidity measurement.[7,8] When the hysteresis exists in measuring systems, the inputs of sensors become unknow in practice since the sensors are usually used to measure various output signals. As a result, the system usually exhibits undesirable inaccuracies or even instability.[9] Large hysteresis is usually observed due to improper interaction between water and porous humidity-sensitive layers.[10] It also causes a mismatch between relative humidity (RH) and the electrical signal during the calibration process.[11] Therefore, the hysteresis issue limits the practical applications of humidity sensors, especially for precision measurement scenarios.

At present, the humidity sensor is developing in the direction of flexibility and light-weighting with the continuous deepening of the research on the inkjet printing patterning technology.[12] Flexible sensors have significant advantages in many aspects such as slenderness, lightness, stretchability, and foldability.[13−18] At the same time, various polymer [polyimide, polyvinyl alcohol (PVA), polymethyl methacrylate, etc.] films and carbon nanomaterials have been developed for humidity sensing because of fast response and high scalability.[19] The characteristic of the high surface-to-volume ratio not only results in their excellent humidity sensing capabilities but also causes their physical and chemical properties extremely susceptible to the environment, usually manifested as a hysteresis phenomenon.[20] Compared with the traditional rigid silicon-based sensor, the hysteresis problem of the emerging and embryonic flexible humidity sensor is more serious, which urgently needs to be paid enough attention to deal with the large-scale commercial application of the flexible humidity sensor.

In recent years, a great deal of efforts has been made to optimize the hysteresis performance of flexible humidity

Received: February 5, 2022
Accepted: April 15, 2022
Published: April 23, 2022

https://doi.org/10.1021/acsomega.2c00743
ACS Omega 2022, 7, 14994−15004

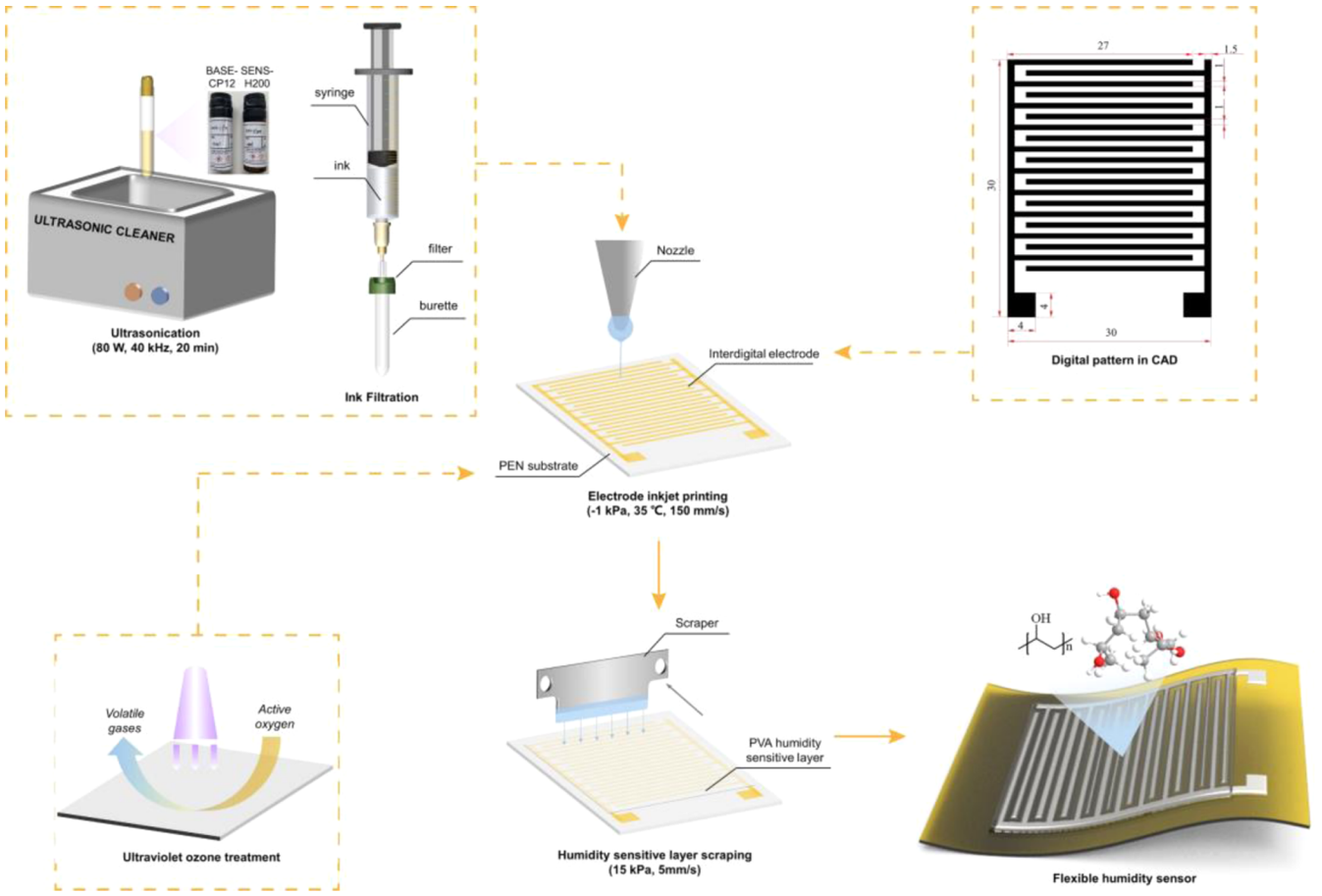

Figure 1. Fabricated flow of the flexible nano silver−PVA humidity sensor.

sensors from the perspective of sensing materials, fabrication technology, and model compensation. To the best of our knowledge, most of the existing research studies have focused on the material innovation and process optimization to reduce the hysteresis; few scholars have established the model of flexible humidity sensor hysteresis to effectively guide and reasonably explain the optimizations. In this work, the flexible nano silver−PVA humidity sensor was fabricated by the inkjet printing technology. The fabricated sensor shows a hysteresis of 2.7% RH in the 12−98% RH range. The hysteresis of the flexible humidity sensor was analyzed in detail from the perspective of the microscopic model and the adsorption−diffusion dynamic model, based on characterization results. We qualitatively analyzed the hysteresis phenomena by dividing the hysteresis microprocess into three continuous stages and concluded that the capillary condensation of water molecules is dominated in the hysteresis of the flexible PVA humidity sensor. The Langmuir monomolecular adsorption dynamic model and Fick diffusion dynamic model were then established, thereby analyzing the adsorption kinetics and diffusion of water molecules, respectively. The corresponding hysteresis optimization strategies were also proposed, such as appropriate pore size and proportion in ink of PVA and diffusion rate of water molecules. This work provides theoretical supports for the hysteresis performance optimization and wider application of high-performance flexible humidity sensors based on PVA.

2. EXPERIMENTAL SECTION

2.1. Materials. The 125 μm thick flexible polyethylene naphthalate (PEN) was used as the substrate. BASE-CP12 solvent-based nano silver conductive ink (silver content of 10 ± 3 wt %) was used for the electrode materials. SENS-H200 ink whose main component is PVA was used to fabricate the humidity-sensitive layer. The above experimental consumables were purchased from Shanghai Mifang Electronic Technology Co., Ltd. Deionized water from Beijing Solarbio Co., Ltd. and 95% ethanol and 99.5% pure acetone from Tianjin Yongda Chemical Reagent Co., Ltd. were serviced as the cleaning solvents for PEN substrates. Lithium chloride, magnesium chloride, sodium bromide, sodium chloride, and potassium sulfate (≥99.7%) were acquired from Tianjin Yongda Chemical Reagent Co., Ltd. and used as received without further purification.

2.2. Sensor Fabrication. Figure 1 shows the preparation process for the flexible nano silver−PVA humidity sensor. MP1100 flexible electronics printer and Dimatix 11610 print nozzle (Shanghai Mifang Electronic Technology Co. Ltd.) were applied for inkjet printing. The electrode layer was prepared under −1 kPa print pressure and 35 °C nozzle temperature. The print and back speed of the nozzle were 150 and 200 mm/s, respectively. The interdigital electrode was then put on the Ansai 946C hot platform (Shenzhen Etechwin Electric Co. Ltd.) for thermal sintering (150 °C, 20 min). The schematic diagram and photograph of the fabricated interdigital electrode are shown in Figure S2a,b. The interdigital electrode shows good flexibility, as shown in

https://doi.org/10.1021/acsomega.2c00743
ACS Omega 2022, 7, 14994−15004

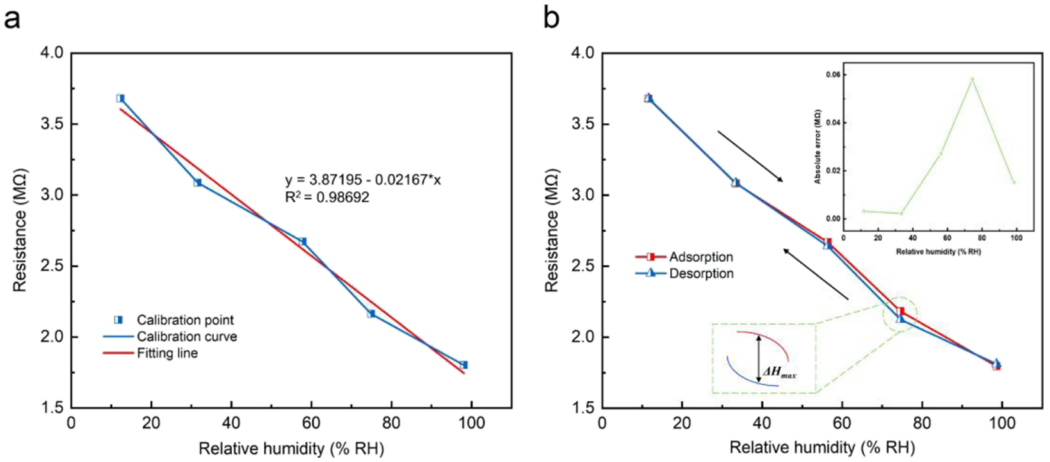

Figure 2. Performance characterization of the flexible nano-silver PVA humidity sensor: (a) calibration curve and (b) hysteresis characteristic curve measured from 12 to 98% RH. The insert shows absolute resistance difference vs RH changes.

Figure S2c. The humidity sensitive layer was prepared by the scraping method. The manufacturing parameters included 33.95 mm scraping height, 5 mm/s scraping speed, and 15 kPa scraping pressure (pre-supplying 20 kPa air pressure for 1000 ms). The SENS-H200 ink was scraped and coated onto the surface of the interdigital electrode, then sintered at 100 °C for 30 min on the hot platform. The fabricated flexible nano silver−PVA humidity sensor is shown in Figure S2d. Resistance of the sensor grew with the rise of the bending angle, as shown in Figure S2e, and the resistance value increased by 0.348% when bending 180°. Overall, the effect of the bending strain on the characteristic of the prepared flexible sensor is negligible due to its high original resistance.

2.3. Testing Setup. The microstructure of the surface of the fabricated flexible humidity sensor was observed with the SMZ680 zoom-stereo microscope (Beijing Jing Bai Zhuo Xian Technology Co. Ltd.). The hysteresis performance and humidity stability of the flexible humidity sensor were characterized with the saturated salt solution method. The temperature and humidity parameters of the reagents used in the test are shown in Table S1. The theoretical framework of the characterization system is shown in Figure S3a. The system was sealed and placed in an LRH-70 incubator (Shanghai Yiheng Scientific Instrument Co. Ltd., 0−60 °C working range, 0.1 °C resolution, ±0.5 °C fluctuation) for 2 h, and 25 °C constant temperature environment was set, as shown in Figure S3b. After reaching the gas−liquid equilibrium phase, the resistance of the flexible humidity sensor was recorded by the signal acquisition module, and the microenvironment humidity evolution was monitored in real time by the humidity monitoring module at the same time. A homemade humidity generator was utilized to test the dynamic response performance of the flexible humidity sensor, as shown in Figure S4.

3. RESULTS AND DISCUSSION

3.1. Sensor Calibration and Hysteresis Analysis. Figure 2a shows the calibration curve of the flexible humidity sensor. It was observed that the resistance of the flexible humidity sensor decreased with the increase in the environmental humidity. The resistance value dropped by about 104.27% as the humidity from 12% RH increased to 98% RH at 25 °C. The sensing mechanism was mainly based on the electrical impedance changes caused by the adsorption and desorption of PVA and water molecules in the air, so as to realize the sensing of humidity. The deeper humidity sensing mechanism will be discussed later. The measured actual characteristic curve was analyzed by linear fitting, and the linear fitting equation was $y = -0.02167x + 3.87195$, which can be considered as the sensitivity of the fabricated sensor (S) is −0.02167 MΩ/% RH. The linear regression coefficient R^2 of the fitting line reached 0.98692; it shows that the resistance of the flexible humidity sensor has a good linear correspondence with the RH. The actual and fitting resistance values of the flexible humidity sensor at different calibration points were compared and analyzed, and the results are shown in Table 1.

Table 1. Linearity of the Fabricated Flexible Humidity Sensor at Different Calibration Points

no.	relative humidity (% RH)	actual resistance (MΩ)	fitting resistance (MΩ)	absolute error (MΩ)	linearity (%)
1	12.3	3.6810	3.6054	0.0756	4.0234
2	31.6	3.0870	3.1872	0.1002	5.3326
3	57.8	2.6720	2.6194	0.0526	2.7994
4	74.9	2.1640	2.2489	0.0849	4.5184
5	98.1	1.8020	1.7461	0.0559	2.9750

Most of the absolute errors were below 0.1 MΩ at different calibration points, and the linearity was about 5.3%. It can be noted that compared with the resistive humidity sensor based on multi-walled carbon nanotubes[21] and the disulfide/graphene oxide flexible humidity sensor[22] reported by the predecessors, the flexible humidity sensor in this paper has smaller nonlinear errors.

The hysteresis performance of the flexible humidity sensor was characterized from 12 to 98% RH. Five different RH environments (12, 32, 58, 75, and 98% RH) were applied to test the resistive response during both the adsorption and desorption processes. It was observed from Figure 2b that the humidity sensor showed almost no hysteresis below 40% RH, and the positive and negative strokes showed good consistency. The insert indicated a slight hysteresis when the humidity was beyond 50% RH, and the maximum hysteresis was observed at 75% RH. The relatively large hysteresis at a high RH may be closely related to the porous structure of PVA material and interaction between water molecules and tiny

https://doi.org/10.1021/acsomega.2c00743
ACS Omega 2022, 7, 14994−15004

Table 2. Summary of the Humidity Sensing Performance for Various Sensors in This Work and Other Reported Studies

sensing material	fabrication process	detection range (% RH)	hysteresis (% RH)	refs
graphene/silver	drop casting	40–98	6	24
polyimide/silver	inkjet printing/ion-exchange	16–90	6.39	25
polylactic acid/titanium dioxide	spin coating	20–90	12	26
reduced graphene oxide/nanodiamond	drop casting	11–97	3.5	23
PVA	inkjet printing/scraping	12–98	2.7	our work

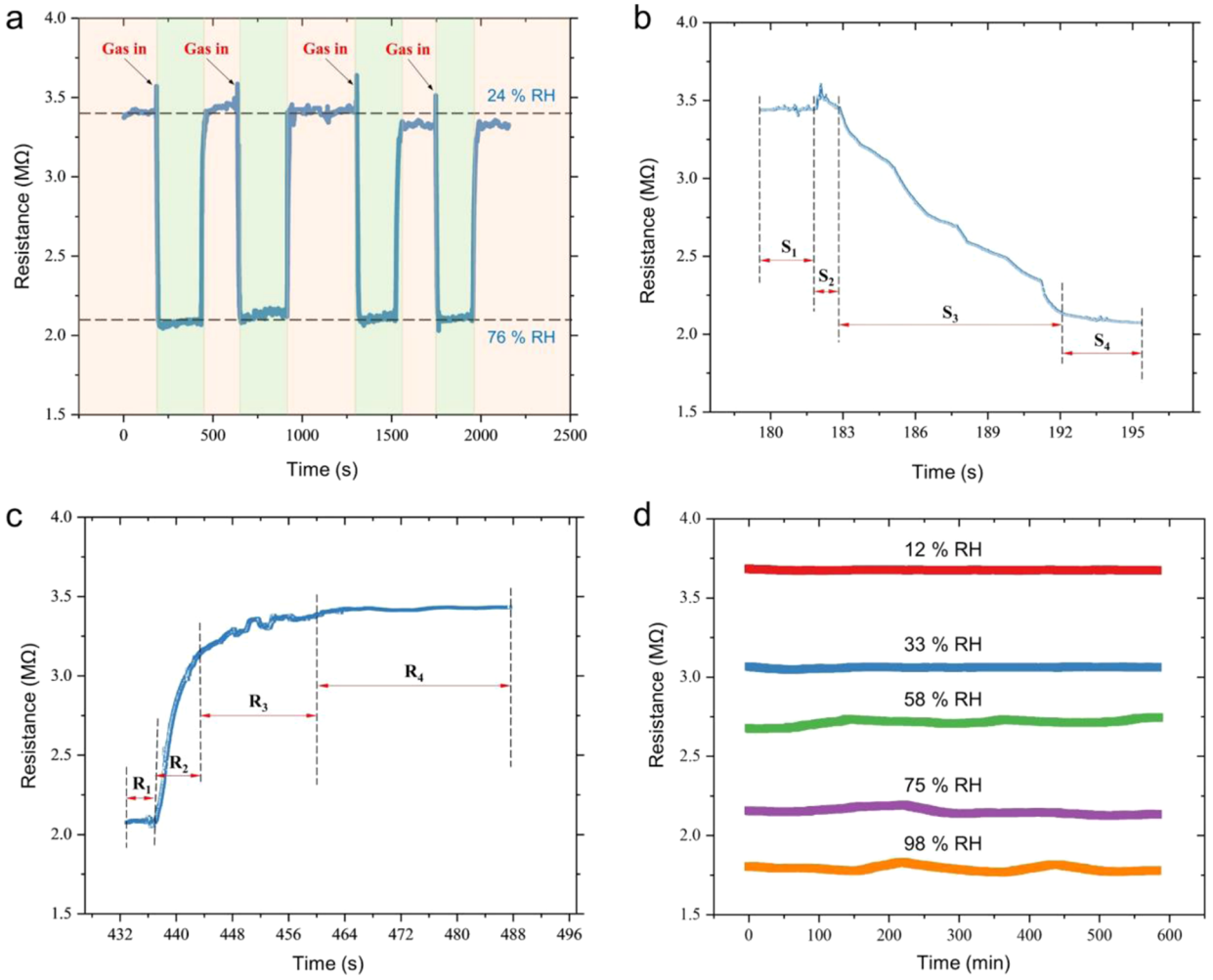

Figure 3. Dynamic characteristics of the flexible nano-silver PVA humidity sensor: (a) repeatability measurement, (b) response property, and (c) recovery property between 24 and 76% RH. (d) Long-term stability of the humidity sensor exposed to 12, 33, 58, 75, and 98% RH.

pores, which will be discussed in the later section. The hysteresis was calculated using the following eq 1,[21,22]

$$H = \frac{\Delta H_{max}}{S} \quad (1)$$

where H is the maximum hysteresis, S is the sensitivity, and ΔH_{max} is the maximum absolute difference of resistance values during the adsorption and desorption processes, for this study, measured at 75% RH.

The maximum hysteresis of the fabricated flexible humidity sensor was 2.7% RH. Table 2 shows the comparison of hysteresis characteristics in the reported literature studies.[23−26] Remarkably, our humidity sensor demonstrated the lowest hysteresis characteristics.

The water molecules and the surface of the humidity sensitive layer interact with each other through hydrogen bonds. The adsorption usually occurs in two ways, physisorption and chemisorption, and physisorption dominates the whole adsorption process in this study. The physisorption has the characteristics of the fast rate, weak force, and easy desorption, which caused the flexible humidity sensor to show short response/recovery time and small hysteresis to RH changes.[27,28]

3.2. Dynamic Characteristics and Stability Characterization. Figure 3a shows the real-time dynamic repeatability test curve of the fabricated flexible nano-silver PVA humidity sensor under the humidity change between 24% RH and 76% RH for four cycles. Obviously, the stable resistance value of the sensor in the two humidity environments basically keeps fluctuating around the baseline. It can be observed that the sensor demonstrates an excellent dynamic characteristic for humidity sensing. Typical humidity detection scenarios such as

https://doi.org/10.1021/acsomega.2c00743
ACS Omega 2022, 7, 14994−15004

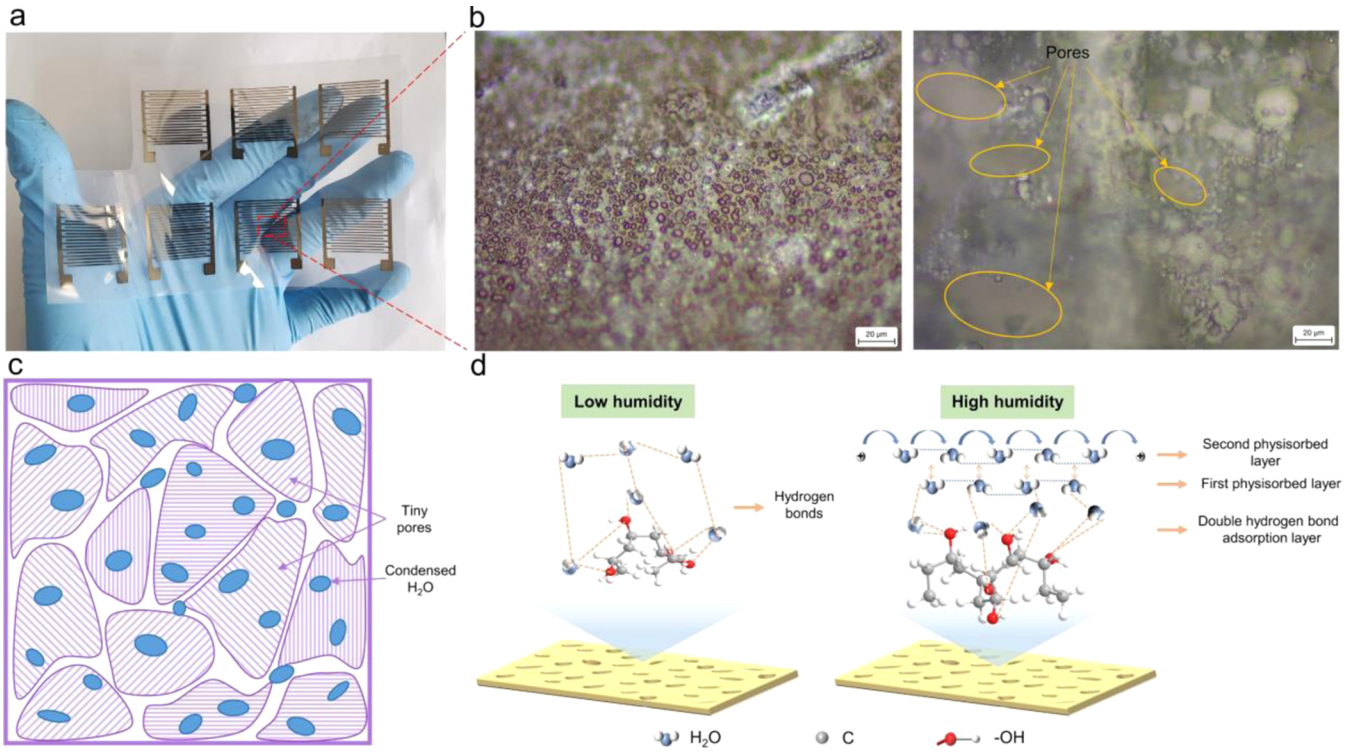

Figure 4. (a) Photograph showing multiple sensors prepared on a PEN substrate. (b) Optical microscopy image and (c) corresponding schematic diagram of the flexible nano silver−PVA humidity sensor. (d) Schematic diagram of the humidity sensing mechanism.

respiration monitoring and microenvironment monitoring in food transportation have placed higher requirements on the response/recovery time of the humidity sensor. As shown in Figure 3b, the humidity response process of the sensor can be divided into four stages. First, the sensor had a stable resistance output value in the low humidity environment (S1 stage), then in the S2 stage, the air in the ventilation hose was first blown out due to the opening of the control valve, causing the output of the sensor to fluctuate. In the S3 stage, the sensor was in contact with an increased number of water molecules, resulting in a rapid decrease in resistance. Eventually, the sensor responded continuously and reached a stable output in the role of moist air (S4). It can be seen that the response time of the prepared humidity sensor is about 9 s, demonstrating the rapid response ability under a wide range of humidity changes. We further explored the recovery characteristics of the sensor and similarly divided the process into four stages. R1 and R2 represent the stable state of the flexible humidity sensor under high and low RH environments, respectively. The sensor was in the rapid and slow recovery status in the R2 and R3 stages and time consuming for 6 and 15 s, where the rapid recovery is the process of recovering 90% of the stable resistance value. In the R3 stage, the decrease in the desorption rate of the humidity sensitive layer contributed to a slower rise of resistance compared to the R2 stage, and the in-depth mechanism will be analyzed in Section 3.4. Table S2 reports few previous studies on the response and recovery time of humidity sensors fabricated by diverse methods. It appears that we have realized the preparation of a fast-response sensor.

Long-term stability is another important parameter of the humidity sensor, which directly determines its service life. The stability of the prepared flexible humidity sensor was tested by the saturated salt solution method in the 25 °C environment. A continuous test was carried out for 10 h under five humidity conditions (12, 33, 58, 75, and 98% RH), and the results are manifested in Figure 3d. Overall, the sensor exhibits acceptable stability under different RH conditions. It is worth noting that the stability of the sensor under lower RH conditions is superior to that under higher RH conditions. Specifically, the output limit difference of the sensor is 0.0729 and 0.0632 MΩ at 98% RH and 75% RH, respectively, while the other three test results are all less than 0.02 MΩ. This may be due to the more intense interfacial interaction between the sensor and the microenvironment under high RH conditions. It can be roughly considered that the stability of the prepared flexible humidity sensor fluctuates greatly under the condition of high RH, but it is still in a satisfactory range in general.

3.3. Humidity Sensing Mechanism. The microstructure characterization of the fabricated flexible humidity sensor helps better understand the sensing mechanism and hysteresis characteristics. The micrographs (Figure 4b) reveal that the humidity sensitive layer material was uniformly adhered to the interdigital electrode, and the surface of the humidity sensitive layer was distributed with many tiny pores with different diameters. Figure 4c shows the layout of the pore structure of the PVA humidity sensitive layer. The water vapor condensed easily due to the capillary action of the tiny pores; therefore, the porous structure can be considered as the active sites in the sensing process.[29] It can be noted that these pores increase the specific surface area of the flexible sensor surface in contact with the outside gas, thus increasing the probability of the humidity sensitive layer surface capturing water molecules in the surrounding environment and improving the sensitivity of the flexible humidity sensor.

The underlying mechanism of water molecules influencing the conductive properties of the PVA humidity sensitive layer is schematically described in Figure 4d. The PVA is a polymer material with tremendous number of hydrophilic functional

https://doi.org/10.1021/acsomega.2c00743
ACS Omega 2022, 7, 14994−15004

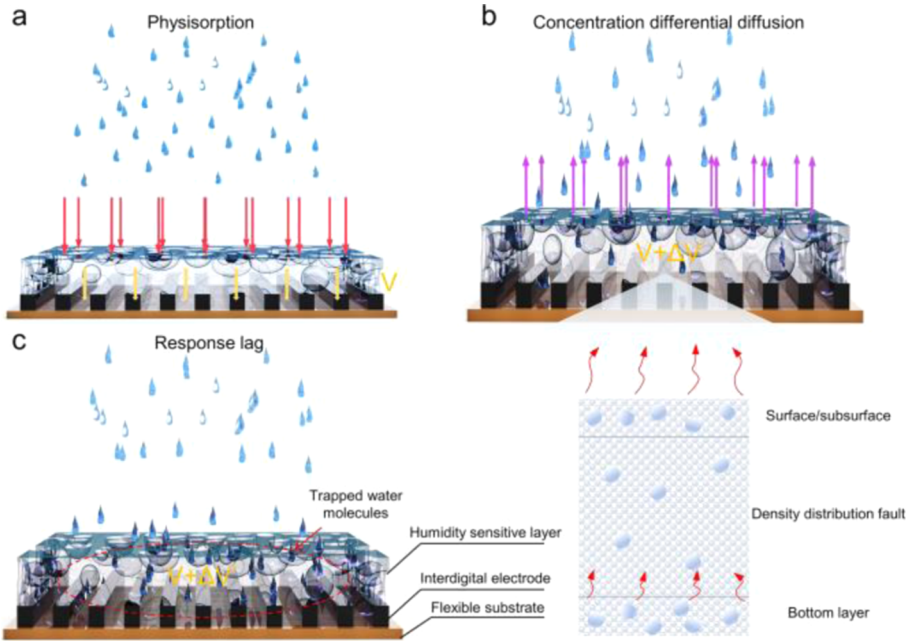

Figure 5. Hysteresis microscopic model. (a) Water molecules are adsorbed by the PVA humidity sensitive layer and causing swelling. (b) Part of the water molecules break away from the humidity sensitive layer. (c) Trapped water molecules caused by capillary condensation eventually lead to the hysteresis of the humidity sensor.

groups (such as hydroxyl) and abundant active sites, as shown in Figure 4a,b. The water molecules nearby were easily captured and adsorbed on the polar groups, which led to an increase in the dielectric constant. The resistance value is inversely proportional to the dielectric constant; hence, the resistance value decreased during the process of adsorption.[27] At low RH, the physisorption between water molecules and hydroxyl groups via double hydrogen bonds first occurred on the surface of the PVA layer.[30] A small number of water molecules captured under the action of hydrogen bonds formed discontinuous layers which would restrict the free movement of water molecules so that high resistance was shown. At the same time, the PVA material was dehydrated to form epoxy groups. Those oxygen-containing functional groups have excellent hydrophilicity and can provide more active sites for adsorption of water molecules.[31] With the increase in RH, water molecules were adsorbed by the PVA layer extensively, and protons derived from ionization of adsorbed water molecules could act as carriers. A large number of charge carriers get accumulated within the host matrix.[32] The hydroxyl groups in PVA were continuously connected via water molecules, and multilayer hydrogen bonds were constructed. According to the Grotthuss chain reactions $[H_3O^+ (H_2O)_n] \rightarrow [H_2O\ H_3O^+ (H_2O)_{n-1}] \rightarrow \cdots \rightarrow [(H_2O)_n\ H_3O^+]$ (n = 1, 2, 3, ⋯), hydrogen ions jumped forward continuously and orderly along the proton wire which is connected by hydrogen bonds, thus increasing the charge carrier mobility significantly.[33,34] As a result, the conductivity of the sensor increased, and the resistance decreased.

Physisorption also has a significant effect on sensor hysteresis: desorption became more difficult due to the formation of a multilayer continuous hydrogen bond network at high RH. On the contrary, the discontinuous water layer formed under low RH exhibited poor stability, and only a small amount of water molecules condensed in the pores on the PVA surface, so that the desorption resistance was small, an external performance for a small hysteresis.

3.4. Hysteresis Microscopic Modeling. The hysteresis process of the flexible humidity sensor can be divided into the adsorption stage, desorption stage, and desorption hysteresis stage, according to the concentration variation of residual water molecules (Figure 5).[35−37]

Adsorption stage I: the water molecules in the micro-environment were captured by the PVA humidity sensitive layer by hydrogen bonds and aggregated on the surface because of the existence of polar groups. Part of the water molecules entered the humidity sensitive layer through the porous structure and continued to pass through the internal porous channels to the bottom of the humidity sensitive layer under the action of thermal motion (Figure 5a). After a period of time, the density of water molecules at each position of the sensitive layer was basically unchanged, that is, the adsorption reached a saturated state, and an equilibrium was formed. In addition, the increased moisture in PVA would cause the volumetric expansion, namely, swelling.[38] This caused a great volume increase in the PVA humidity sensitive layer, specifically, from V to $V + \Delta V$.[35]

Desorption stage II: as the water molecules outside the PVA humidity sensitive layer decreased, the internal−external density balance of water molecules was broken, and the internal water molecules began to regulate accordingly. The water molecules on the surface and subsurface quickly escaped from the adsorption of the sensitive layer and diffused into the microenvironment due to the concentration differential diffusion and weak feature of physisorption, as shown in Figure 5b.

Desorption hysteresis stage III: the water molecules in the porous structure and bottom of the sensitive layer first moved toward the surface from the entangled complex porous channels, which was similar to the movement in the capillaries. These water molecules moved to the surface of the sensitive

https://doi.org/10.1021/acsomega.2c00743
ACS Omega 2022, 7, 14994−15004

layer and then diffused into the environment. The desorption time was longer than that of the surface or subsurface, thus generating a density distribution fault in the middle of the sensitive layer. Besides, the increased volume of the PVA layer would inevitably lead to a large desorption resistance of water molecules in the deeper layer, which explained the recovery time of the sensor far exceeding the response time. Although the RH outside the humidity sensitive layer decreased, there was still a certain amount of residual water molecules (Figure 5c). Overall, the volume recovery of PVA from swelling remained incomplete ($V + \Delta V'$), resulting in a resistance response lag and longer recovery time. It can be considered that the capillary condensation of water molecules in the PVA humidity sensitive layer is the main factor for the hysteresis of the sensor.[35]

3.5. Hysteresis Dynamic Modeling. The qualitative analysis of hysteresis phenomenon was presented in the above section, the quantitative modeling aimed at hysteresis was subsequently discussed from the perspective of the theoretical dynamics, and the corresponding hysteresis optimization strategies were also proposed. When the concentration of external water molecules is constant (i.e., the RH is constant), the water molecules are transported to the surface of the humidity sensitive layer under the action of surface force and then are adsorbed. The initial adsorption rate closely corresponds to the maximum mass transfer rate of the substrate. As the adsorption capacity increases, it is gradually difficult for water molecules to find adsorption sites, so the adsorption rate begins to decline and finally tends to zero at saturation. Since there are multiple degrees of freedom in PVA polymers, the adsorption process is accompanied by an attachment reconfirmation change in the surface substances. Under the influence of water molecules, the original humidity sensitive layer may undergo attachment reconfirmation change, which has been verified in the related literature.[38,39]

The adsorption probability depends not only on the concentration of adsorbed water molecules but also on the structural phase change between water molecules and PVA humidity sensitive layer material. Although a small amount of PVA dehydration reaction occurs in the humidity sensitive layer to form epoxy groups, most of them still belong to the category of reversible physisorption. The adsorption capacity per unit area of the humidity sensitive layer is limited, and the molecular force between the humidity sensitive layer and water molecules decreases rapidly as the distance increases, so we can simplify the model to a monolayer adsorption type. Therefore, the adsorption kinetics of the humidity sensitive layer to water molecules in the air can be explained by the Langmuir monomolecular adsorption dynamic model.[40] The basic assumption is as follows: water molecules are uniformly adsorbed on the surface of the PVA humidity sensitive layer through monolayer adsorption, and there is no interaction between the adsorbed water molecules. All the adsorption sites on the surface of the humidity sensitive layer have the same adsorption force. The model is expressed by eq 2

$$\frac{C_e}{Q_e} = \frac{1}{bQ_m} + \frac{C_e}{Q_m} \tag{2}$$

where C_e is the equilibrium partial pressure of water molecules in the gas phase, b is the Langmuir constant, which is the ratio of adsorption and desorption rate constant of the PVA humidity sensitive layer, and Q_e and Q_m are the volume of adsorbed water molecules in the standard state and the maximum volume of water molecules that can be adsorbed through monolayer adsorption by the PVA humidity sensitive layer, respectively.

Equation 1 shows that the plot of (C_e/Q_e) versus C_e should yield a straight line if the adsorption equilibrium follows the Langmuir equation. The values of Q_m and b can be derived from the slope and intercept of the line. Therefore, the dimensionless equilibrium parameter R_L, also known as separation factor, is given on the basis of eq 2

$$R_L = \frac{1}{1 + bC_0} \tag{3}$$

where the humidity sensitive layer has a good adsorption effect on water molecules if the value of R_L is between 0 and 1, while $R_L > 1$ indicates an unfavorable adsorption. The adsorption is linear if $R_L = 1$, while $R_L = 0$ indicates irreversible adsorption.[40] According to the adsorption dynamic model of the flexible humidity sensor mentioned above, the performance of the flexible humidity sensor can be optimized by adjusting the equilibrium partial pressure, the maximum adsorption capacity of PVA to water molecules.

When there is a concentration gradient of water molecules inside and outside the PVA humidity sensitive layer, water molecules will diffuse from high to low concentration area under the action of thermal movement, and the redistribution of water molecules will continue until the equilibrium. According to Fick's first law, the flow rate of the diffusible substance passing through a unit cross-sectional area perpendicular to the diffusion direction per unit time (called the diffusion flux) is proportional to the concentration gradient at the cross-section, which is calculated using eq 4

$$J = -D\frac{\partial C(x, t)}{\partial x} \tag{4}$$

where J is the diffusion flux, C is the volume concentration of water molecules in the microenvironment, assuming it is only a function of x and t, x and t are the distance coordinate of the diffusion direction of water molecules ($x = 0$ represents the surface of the humidity sensitive layer, and the direction of internal diffusion is positive) and the diffusion time, respectively, and D is the diffusion coefficient. The equation indicates that the local diffusion rate of water molecules in the humidity sensitive layer per unit area is proportional to the concentration gradient of water molecules, and the proportional constant is defined as the diffusion coefficient of water molecules. The negative sign in the equation means that the diffusion direction of water molecules is the opposite direction of the concentration gradient. According to the law of conservation of matter, variation of the water molecule concentration in the microenvironment must be equal to the decrease in the diffusion flux, that is

$$\frac{\partial C(x, t)}{\partial t} = -\frac{\partial J(x, t)}{\partial x} \tag{5}$$

Substituting eq 4 into eq 5, Fick's second diffusion law in the one-dimensional form is obtained, as follows

$$\frac{\partial C(x, t)}{\partial t} = \frac{\partial}{\partial x}\left[D\frac{\partial C(x, t)}{\partial x}\right] \tag{6}$$

According to Fick's second diffusion law, the complete solution of the equation can be obtained under certain

https://doi.org/10.1021/acsomega.2c00743
ACS Omega 2022, 7, 14994−15004

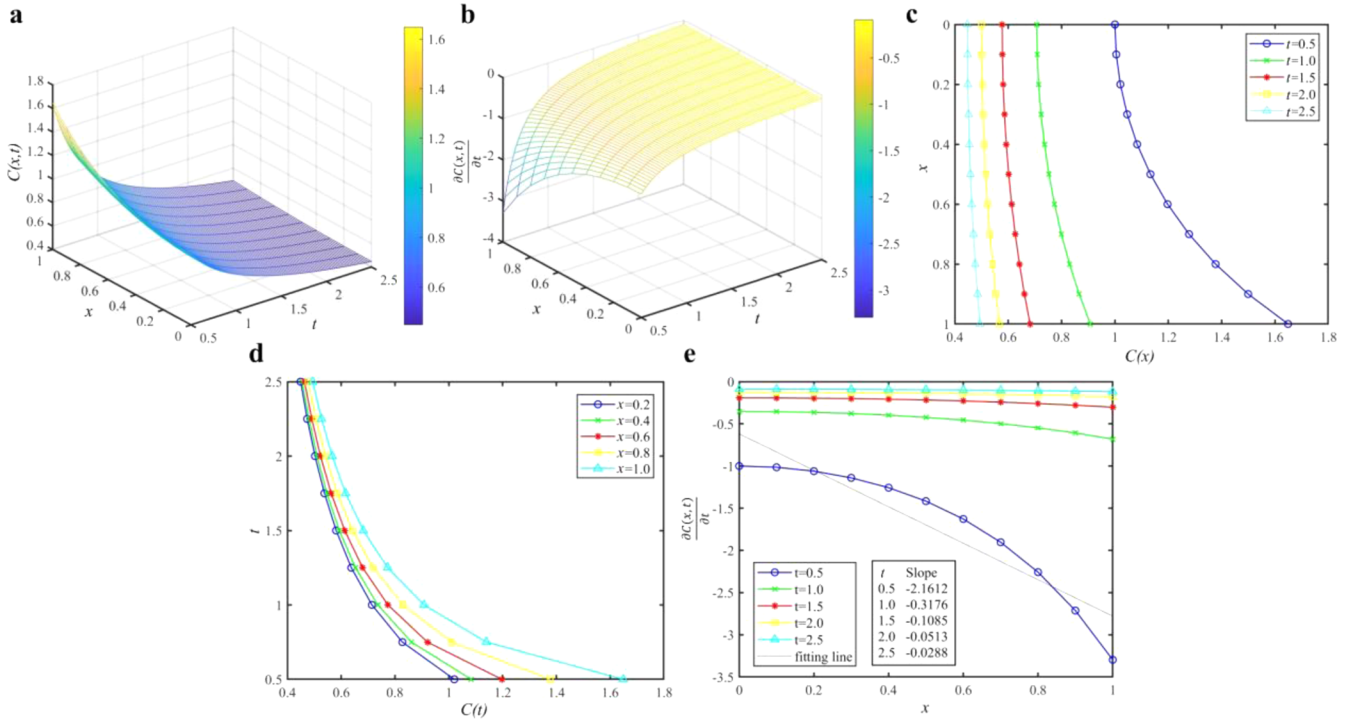

Figure 6. 3D graph of (a,b) water molecule concentrate (C) and diffusion rate under different diffusion depth (x varies from 0 to 1) and time (t varies from 0.5 to 2.5). (c) C vs x with t of 0.5, 1.0, 1.5, 2.0, and 2.5, respectively. (d) C vs t with diffusion depth of 0.2, 0.4, 0.6, 0.8, and 1.0, respectively. (e) Water molecule diffusion rate vs diffusion depth with diffusion time of 0.5, 1.0, 1.5, 2.0, and 2.5, respectively. The insert shows the linear fitting result.

boundary conditions. The background for solving the first type of Fick's law is that the water molecules in the microenvironment are transported to the surface of the PVA humidity sensitive layer of the flexible humidity sensor and gradually diffuse into it. It can be considered that the water molecules in the microenvironment maintain a constant concentration. The boundary conditions are

$$C(0, t) = C_s \text{ and } C(\infty, t) = 0 \tag{7}$$

The first solution of Fick's second law satisfying the above boundary conditions is as follows

$$C(x, t) = C_s erfc\left[\frac{x}{2\sqrt{Dt}}\right] \tag{8}$$

where C_S and $\sqrt{(Dt)}$ are the constant concentration of water molecules and the diffusion length, respectively. From the first solution of Fick's law, it can be seen that the water molecule concentration distribution on the surface and subsurface of the humidity sensitive layer conforms to the residual error function ($erfc$) distribution, that is, the redistribution diffusion occurs, and the diffusion continues inside the humidity sensitive layer. In this case, the concentration of water molecules in the diffusion process can be regarded as constant. Assuming that the total amount of water molecules participating in the redistribution diffusion is S, the concentration of water molecules on the surface of the humidity sensitive layer is C_{sub}. The boundary conditions are as follows

$$\int_0^\infty C(x, t)\, dx = S \text{ and } C(x, \infty) = 0 \tag{9}$$

The second solution of Fick's second law satisfying the above boundary conditions is as follows

$$C(x, t) = \frac{S}{\sqrt{\pi Dt}} \exp\left[\frac{x^2}{4Dt}\right] \tag{10}$$

It can be noted from eq 10 that the redistribution concentration of water molecules in the humidity sensitive layer of the flexible humidity sensor obeys the Gaussian distribution, and the distribution of water molecules moves with the extension of time. In order to simplify the diffusion model, the coefficient of the exponential function when $t = 0.5$ in eq 10 and diffusion coefficient D were set to unity, so as to realize normalization. Figure 6 shows the relationships among C and its partial derivation to t versus parameter x and t based on the simplified mathematical model. Notably, the five parameter values were selected to make the image more contrast. As can be seen from Figure 6a,c the concentration of water molecules increased with the increase in the diffusion depth, which confirmed the occurrence of redistribution diffusion. It can be observed from Figure 6d that the concentration of water molecules in each layer of PVA showed a decreasing trend with the extension of the diffusion time. The concentration of water molecules in the surface and subsurface decreased more slowly than that in the deeper layer due to concentration difference. Remarkably, the concentration of water molecules dropped to almost the same level at $x = 0.2-1.0$ when $t = 2.5$, indicating the aggregation of water molecules in a deeper layer of PVA, which undoubtedly contributing to the capillary condensation. Figure 6b,e shows the partial derivation of C to t (i.e., diffusion rate) versus diffusion time and depth. The color bar of the three-dimensional (3D) surface indicated that the faster diffusion rate was concentrated at greater depth and shorter time. A polynomial fitting was performed on the relationship curve between the diffusion rate and diffusion depth (Figure 6e). The fitting slope increased

https://doi.org/10.1021/acsomega.2c00743
ACS Omega 2022, 7, 14994−15004

sharply when t increased from 0.5 to 1.0 and then stabilized, indicating that the diffusion of water molecules is restricted by time and concentrated within t = 1.0. The trend of the curve depicted that the diffusion resistance of water molecules in the deep layer of PVA was small, thus inducing the occurrence of sensor hysteresis, which may be due to the coupling control effect of adsorption and diffusion on the surface. Therefore, it is necessary to control the redistribution diffusion time and concentration of water molecules at different depths in the PVA layer to weaken the influence of water molecular density distribution fault in the desorption process and to achieve a balance between sensing and hysteresis.

According to the establishment and analysis of the above Fick diffusion model, it can be seen that the hysteresis characteristic of the flexible PVA humidity sensor can be optimized by adjusting the diffusion coefficient and time of water molecules in PVA. Simultaneously, the hysteresis effect is composed of the adsorption−desorption equilibrium and the diffusion kinetics of water molecules in the porous humidity sensitive layer. Porous structure of PVA humidity sensitive increases the effective humidity sensitive area on the surface of the flexible humidity sensitive layer, so as to increase the probability of capturing water molecules in the microenvironment and the sensitivity of the flexible humidity sensor. However, the existence of the porous structure will also increase the hysteresis. It is one of the important directions for further research to explore the optimal PVA material ratio to reach the appropriate pore size and the adsorption−desorption rate ratio of the humidity sensitive layer, thus achieving the balance between sensitivity and hysteresis.

4. CONCLUSIONS

In this work, a flexible nano silver−PVA humidity sensor was fabricated with inkjet printing and coating technologies. The statics calibration and hysteresis characterization of the flexible humidity sensor were tested from 12 to 98% RH range using the saturated salt solution method. It was observed that the sensor resistance dropped by about 104.27% in total as the RH increased due to the construction of the continuous hydrogen bond network and the occurrence of Grotthuss chain reactions. The flexible sensor exhibits salient features including a high sensitivity of −0.02167 MΩ/% RH, linearity of 5.3%, and low hysteresis of 2.7% RH, making it suitable for numerous humidity detection applications. The sensor also displays fast dynamic response and recovery characteristics (response/recovery times of 9/21 s), which are advantageous in polymer-based humidity sensors. However, it is noted that the recovery and hysteresis characteristics of the nano silver−PVA humidity sensor still have room for improvement.

Hysteresis characteristic of the flexible humidity sensor was thoroughly analyzed from the perspectives of the microscopic process and dynamic model. It can be noted that the capillary condensation of water molecules in the porous microstructure of the PVA humidity sensitive layer is the main reason of the hysteresis. The hysteresis is controlled by the coupling of adsorption and diffusion of water molecules in the humidity sensitive layer. The adsorption kinetics was based on the Langmuir monomolecular adsorption dynamic model, and the proposed separation factor can effectively evaluate the adsorption effect. The diffusion process was analyzed by setting boundary conditions and solving Fick's law, and the distribution law of water molecule volume concentration was obtained. The results demonstrated the occurrence of the redistribution diffusion and low diffusion resistance of water molecules in the deep layer of PVA. Future work could be focused on optimizing the diffusion rate and PVA material ratio, thereby achieving the balance between high sensitivity and low hysteresis.

■ ASSOCIATED CONTENT

Supporting Information

The Supporting Information is available free of charge at https://pubs.acs.org/doi/10.1021/acsomega.2c00743.

Equilibrium temperature and RH corresponding to different saturated salt solutions; comparison of response and recovery time of various humidity sensors; contact angle measurements of flexible substrates; photograph and bending reliability of the fabricated flexible nano silver−PVA humidity sensor; homemade test system of sensor calibration and hysteresis characterization; and humidity generator for sensor dynamic performance testing (PDF)

■ AUTHOR INFORMATION

Corresponding Author

Xiaoshuan Zhang − *College of Engineering, China Agricultural University, Beijing 100083, China;* orcid.org/0000-0002-0395-928X; Email: zhxshuan@cau.edu.cn

Authors

Jie Xia − *College of Engineering, China Agricultural University, Beijing 100083, China*

Xuepei Wang − *College of Engineering, China Agricultural University, Beijing 100083, China; School of Electronic Information and Electrical Engineering, Shanghai Jiao Tong University, Shanghai 200240, China*

Xiang Wang − *College of Engineering, China Agricultural University, Beijing 100083, China*

Krisztina Majer-Baranyi − *Food Science Research Group, Institute of Food Science and Technology, Hungarian University of Agriculture and Life Sciences, Budapest H-1022, Hungary*

Complete contact information is available at: https://pubs.acs.org/10.1021/acsomega.2c00743

Author Contributions

‖J.X. and X.W. contributed equally to this work.

Notes

The authors declare no competing financial interest.

■ ACKNOWLEDGMENTS

The authors gratefully acknowledge the financial support from the National Natural Science Foundation of China (grant number: 32071917) and the Key Laboratory of Storage of Agricultural Products, Ministry of Agriculture and Rural Affairs (grant number: Kf202008).

■ REFERENCES

(1) Zhang, X.; Cui, H.; Gui, Y.; Tang, J. Mechanism and Application of Carbon Nanotube Sensors in SF6 Decomposed Production Detection: A Review. *Nanoscale Res. Lett.* **2017**, *12*, 177.

(2) Yang, Y.; Deng, Z. D. Stretchable Sensors for Environmental Monitoring. *Appl. Phys. Rev.* **2019**, *6*, 011309.

(3) Neethirajan, S.; Kemp, B. Digital Livestock Farming. *Sens. Bio-Sens. Res.* **2021**, *32*, 100408.
(4) Chung, M.; Fortunato, G.; Radacsi, N. Wearable Flexible Sweat Sensors for Healthcare Monitoring: A Review. *J. R. Soc., Interface* **2019**, *16*, 20190217.
(5) Nag, A.; Mukhopadhyay, S. C.; Kosel, J. Wearable Flexible Sensors: A Review. *IEEE Sens. J.* **2017**, *17*, 3949−3960.
(6) Mamun, M. A. A.; Yuce, M. R. Sensors and Systems for Wearable Environmental Monitoring Toward IoT-Enabled Applications: A Review. *IEEE Sens. J.* **2019**, *19*, 7771−7788.
(7) Islam, T.; Saha, H. Hysteresis Compensation of a Porous Silicon Relative Humidity Sensor Using ANN Technique. *Sens. Actuators, B* **2006**, *114*, 334−343.
(8) Wang, X.; Zhang, M.; Zhang, L.; Xu, J.; Xiao, X.; Zhang, X. Inkjet-printed flexible sensors: From function materials, manufacture process, and applications perspective. *Mater. Today Commun.* **2022**, *31*, 103263.
(9) Chen, X.; Feng, Y.; Su, C.-Y. Adaptive Control for Continuous-Time Systems with Actuator and Sensor Hysteresis. *Automatica* **2016**, *64*, 196−207.
(10) Fürjes, P.; Kovács, A.; Dücsö, Cs.; Ádám, M.; Müller, B.; Mescheder, U. Porous Silicon-Based Humidity Sensor with Interdigital Electrodes and Internal Heaters. *Sens. Actuators, B* **2003**, *95*, 140−144.
(11) Lee, S.-W.; Choi, B. I.; Kim, J. C.; Woo, S.-B.; Kim, Y.-G.; Kwon, S.; Yoo, J.; Seo, Y.-S. Sorption/Desorption Hysteresis of Thin-Film Humidity Sensors Based on Graphene Oxide and Its Derivative. *Sens. Actuators, B* **2016**, *237*, 575−580.
(12) Khan, S.; Lorenzelli, L.; Dahiya, R. S. Technologies for Printing Sensors and Electronics Over Large Flexible Substrates: A Review. *IEEE Sens. J.* **2015**, *15*, 3164−3185.
(13) Deng, W.-J.; Wang, L.-F.; Dong, L.; Huang, Q.-A. Experimental Study of the Bending Effect on LC Wireless Humidity Sensors Fabricated on Flexible PET Substrates. *J. Microelectromech. Syst.* **2018**, *27*, 761−763.
(14) Qian, C.; Li, L.; Gao, M.; Yang, H.; Cai, Z.; Chen, B.; Xiang, Z.; Zhang, Z.; Song, Y. All-Printed 3D Hierarchically Structured Cellulose Aerogel Based Triboelectric Nanogenerator for Multi-Functional Sensors. *Nano Energy* **2019**, *63*, 103885.
(15) Morais, R. M.; Klem, M. d. S.; Nogueira, G. L.; Gomes, T. C.; Alves, N. Low Cost Humidity Sensor Based on PANI/PEDOT:PSS Printed on Paper. *IEEE Sens. J.* **2018**, *18*, 2647−2651.
(16) Wang, Y.; Zhang, L.; Zhang, Z.; Sun, P.; Chen, H. High-Sensitivity Wearable and Flexible Humidity Sensor Based on Graphene Oxide/Non-Woven Fabric for Respiration Monitoring. *Langmuir* **2020**, *36*, 9443−9448.
(17) Xu, K.; Lu, Y.; Takei, K. Multifunctional Skin-Inspired Flexible Sensor Systems for Wearable Electronics. *Adv. Mater. Technol.* **2019**, *4*, 1800628.
(18) Zhang, M.; Wang, X.; Feng, H.; Huang, Q.; Xiao, X.; Zhang, X. Wearable Internet of Things Enabled Precision Livestock Farming in Smart Farms: A Review of Technical Solutions for Precise Perception, Biocompatibility, and Sustainability Monitoring. *J. Cleaner Prod.* **2021**, *312*, 127712.
(19) Yuan, W.; Shi, G. Graphene-Based Gas Sensors. *J. Mater. Chem. A* **2013**, *1*, 10078.
(20) Anichini, C.; Aliprandi, A.; Gali, S. M.; Liscio, F.; Morandi, V.; Minoia, A.; Beljonne, D.; Ciesielski, A.; Samorì, P. Ultrafast and Highly Sensitive Chemically Functionalized Graphene Oxide-Based Humidity Sensors: Harnessing Device Performances via the Supramolecular Approach. *ACS Appl. Mater. Interfaces* **2020**, *12*, 44017−44025.
(21) Kondalkar, V. V.; Ryu, G.; Lee, Y.; Lee, K. Development of Highly Sensitive and Stable Humidity Sensor for Real-Time Monitoring of Dissolved Moisture in Transformer-Insulating Oil. *Sens. Actuators, B* **2019**, *286*, 377−385.
(22) Qiang, T.; Wang, C.; Liu, M.-Q.; Adhikari, K. K.; Liang, J.-G.; Wang, L.; Li, Y.; Wu, Y.-M.; Yang, G.-H.; Meng, F.-Y.; Fu, J.-H.; Wu, Q.; Kim, N.-Y.; Yao, Z. High-Performance Porous MIM-Type Capacitive Humidity Sensor Realized via Inductive Coupled Plasma and Reactive-Ion Etching. *Sens. Actuators, B* **2018**, *258*, 704−714.
(23) Yu, X.; Chen, X.; Ding, X.; Chen, X.; Yu, X.; Zhao, X. High-Sensitivity and Low-Hysteresis Humidity Sensor Based on Hydrothermally Reduced Graphene Oxide/Nanodiamond. *Sens. Actuators, B* **2019**, *283*, 761−768.
(24) Rahim, I.; Shah, M.; Khan, A.; Luo, J.; Zhong, A.; Li, M.; Ahmed, R.; Li, H.; Wei, Q.; Fu, Y. Capacitive and Resistive Response of Humidity Sensors Based on Graphene Decorated by PMMA and Silver Nanoparticles. *Sens. Actuators, B* **2018**, *267*, 42−50.
(25) Yang, T.; Yu, Y. Z.; Zhu, L. S.; Wu, X.; Wang, X. H.; Zhang, J. Fabrication of Silver Interdigitated Electrodes on Polyimide Films via Surface Modification and Ion-Exchange Technique and Its Flexible Humidity Sensor Application. *Sens. Actuators, B* **2015**, *208*, 327−333.
(26) Mallick, S.; Ahmad, Z.; Touati, F.; Bhadra, J.; Shakoor, R. A.; Al-Thani, N. J. J. PLA-TiO2 Nanocomposites: Thermal, Morphological, Structural, and Humidity Sensing Properties. *Ceram. Int.* **2018**, *44*, 16507−16513.
(27) Zhang, D.; Zong, X.; Wu, Z. Fabrication of Tin Disulfide/Graphene Oxide Nanoflower on Flexible Substrate for Ultrasensitive Humidity Sensing with Ultralow Hysteresis and Good Reversibility. *Sens. Actuators, B* **2019**, *287*, 398−407.
(28) Karunarathne, T. S. E. F.; Wijesinghe, W. P. S. L.; Rathuwadu, N. P. W.; Karalasingam, A.; Manoharan, N.; Sameera, S. A. L.; Sandaruwan, C.; Amaratunga, G. A.; de Silva, S. G. M. Fabrication and Characterization of Partially Conjugated Poly (Vinyl Alcohol) Based Resistive Humidity Sensor. *Sens. Actuators, A* **2020**, *314*, 112263.
(29) Singh, H.; Kumar, A.; Bansod, B. S.; Singh, T.; Thakur, A.; Singh, T.; Sharma, J. Enhanced Moisture Sensing Properties of a Nanostructured ZnO Coated Capacitive Sensor. *RSC Adv.* **2018**, *8*, 3839−3845.
(30) Tripathy, A.; Sharma, P.; Sahoo, N.; Pramanik, S.; Abu Osman, N. A. Moisture Sensitive Inimitable Armalcolite/PDMS Flexible Sensor: A New Entry. *Sens. Actuators, B* **2018**, *262*, 211−220.
(31) Liu, B.; Sun, H.; Peng, T.; Yang, J.; Ren, Y.; Ma, J.; Tang, G.; Wang, L.; Huang, S. High Selectivity Humidity Sensors of Functionalized Graphite Oxide with More Epoxy Groups. *Appl. Surf. Sci.* **2020**, *503*, 144312.
(32) Khasim, S.; Pasha, A.; Badi, N.; Lakshmi, M.; Al-Ghamdi, S. A.; AL-Aoh, H. A. PVA Treated PEDOT-PSS: TiO2 Nanocomposite Based High-Performance Sensors Towards Detection of Relative Humidity and Soil Moisture Content for Agricultural Applications. *J. Polym. Environ.* **2021**, *29*, 612−623.
(33) Jang, J. H.; Han, J. I. Cylindrical Relative Humidity Sensor Based on Poly-Vinyl Alcohol (PVA) for Wearable Computing Devices with Enhanced Sensitivity. *Sens. Actuators, A* **2017**, *261*, 268−273.
(34) Meng, W.; Wu, S.; Wang, X.; Zhang, D. High-Sensitivity Resistive Humidity Sensor Based on Graphitic Carbon Nitride Nanosheets and Its Application. *Sens. Actuators, B* **2020**, *315*, 128058.
(35) Li, W.; Xu, F.; Sun, L.; Liu, W.; Qiu, Y. A Novel Flexible Humidity Switch Material Based on Multi-Walled Carbon Nanotube/Polyvinyl Alcohol Composite Yarn. *Sens. Actuators, B* **2016**, *230*, 528−535.
(36) Fei, T.; Zhao, H.; Jiang, K.; Zhou, X.; Zhang, T. Polymeric Humidity Sensors with Nonlinear Response: Properties and Mechanism Investigation. *J. Appl. Polym. Sci.* **2013**, *130*, 2056−2061.
(37) Papancea, A.; Valente, A. J. M.; Patachia, S. Diffusion and Sorption Studies of Dyes through PVA Cryogel Membranes. *J. Appl. Polym. Sci.* **2010**, *115*, 1445−1453.
(38) Krumova, M.; López, D.; Benavente, R.; Mijangos, C.; Pereña, J. M. Effect of Crosslinking on the Mechanical and Thermal Properties of Poly(Vinyl Alcohol). *Polymer* **2000**, *41*, 9265−9272.
(39) Dijt, J. C.; Stuart, M. A. C.; Hofman, J. E.; Fleer, G. J. Kinetics of Polymer Adsorption in Stagnation Point Flow. *Colloids Surf.* **1990**, *51*, 141−158.
(40) Zhang, Y.; Li, Y.; Yang, L. Q.; Ma, X. J.; Wang, L. Y.; Ye, Z. F. Characterization and Adsorption Mechanism of Zn2+ Removal by

https://doi.org/10.1021/acsomega.2c00743
ACS Omega 2022, 7, 14994−15004

PVA/EDTA Resin in Polluted Water. *J. Hazard. Mater.* **2010**, *178*, 1046−1054.

https://doi.org/10.1021/acsomega.2c00743
ACS Omega 2022, 7, 14994−15004